

Performance Analysis of 5G Cooperative-NOMA for IoT-Intermittent Communication

Imran Khan

Department of Electrical Engineering, University of Engineering and Technology Peshawar, Pakistan
imran_khan@uetpeshawar.edu.pk

Abstract: Non-orthogonal multiple Access (NOMA) is a potential 5G era multiple-access scheme that is proposed for the future mobile Internet and IoT applications which will require enormous increase in data traffic, massive-number of devices connectivity, high spectral efficiency, low-overhead and low-latency. It utilizes the same time-slots, frequency and spreading-codes for all the users. It uses the power-domain and assign different power levels to users for multiple access. The uplink (UL) communication in the present 4G-Networks is performed by the base station (BS) that uses a request-grant mechanism in which a large-overhead and latency is produced. This issue will get more severe in upcoming 5G-Networks. For this purpose, a grant-free NOMA for UL communication, in which dynamic compressed-sensing (DCS) algorithm will perform multi-user detection (MUD) as well as data-detection is proposed. It deploys the temporal-correlation of active-user sets (AUS) in adjacent time-slots from which the estimated AUS is used as the prior-knowledge to estimate AUS in the next time-slot. For the downlink (DL) communication, the proposed system performance evaluation is performed using Rician fading-channels for Cooperative Relaying System (CRS) NOMA. The simulations results show that the proposed DCS-MUD and CRS NOMA over Rician fading-channels perform much better than the conventional CS-MUD and traditional-CRS.

Keywords: 5G, NOMA, IoT, DCS, Cooperative Relaying.

1. Introduction

Internet of things (IoT) is a global network of physical and virtual 'things' that are connected to the Internet [1]. Multiple access scheme is the key technology in the history of wireless communication to distinguish all generations from 1G to 4G. The conventional orthogonal multiple access (OMA) schemes, such as frequency-division multiple access (FDMA), time-division multiple access (TDMA), code-division multiple access (CDMA) and orthogonal frequency-division multiple access (OFDMA) deploy reserved and limited resources for dedicated users which are orthogonal and uniquely allocated. As the frequency-division multiple access (FDMA) is used for 1G which assign frequency bands to each user. The time-division multiple access (TDMA) is used mostly for 2G and GSM which assign time-slots to users. The code-division multiple access (CDMA) is used in 3G which assign channel-codes to users. The orthogonal frequency-division multiple access (OFDMA) is used for current 4G communication networks. All these schemes assign orthogonal resources to the corresponding users in order to eliminate inter-user interference. Currently, all cellular-networks uses such OMA-schemes but none of them can fulfill the explosive demands for future 5G radio access. According to a survey conducted by the International Telecommunication Union (ITU), the data capacity used by the smartphone users is 5% more than the standard phone users [2]. Mobile data traffic is becoming more dominant due

to the increasing usage of mobile devices and proliferation of IoT [3].

To cope with these demands, non-orthogonal multiple access (NOMA) scheme is proposed as the 5G radio access technology for the wireless mobile networks to efficiently utilize the bandwidth, support numerous number of users or nodes, provide low-overhead transmission, better user-fairness, enhanced cell-edge throughput, freedom from request-grant scheduling for connection establishment, improved QoS, and enable low-latency communication [4]. It uses the concept of non-orthogonality which is obtained by using the power-domain. The power-domain can work in either, time, frequency or code domains for performing user-multiplexing at the transmitter (Tx) side [5]. The user-demultiplexing is performed by a large power-difference allocation among the users which mean different power levels to different users and then using multi-user detection (MUD) algorithm such as the successive interference cancellation (SIC) is used at the receiver (Rx) side. It uses the same spectrum for all user equipment (UE) which is possible by using superposition-coding (SC) at the Tx and SIC at the Rx. The superposition is performed by the Tx which superimpose all the individual information signals to a single signal. The SIC algorithm at the Rx perform the reverse of superposition and it decodes the signals one-by-one until obtaining the required signal for intended user. It decodes the strongest and powerful signal at first by treating other signals as noise, and then it subtracts this most powerful signal from the received signal and this process is continued until the required signal for the intended user is obtained by such iteration-mechanism. The basic idea of NOMA scheme is pictorially illustrated in Figure 1 for single BS and two-UEs. It is also compared with conventional OMA Schemes to show the advantages of NOMA over OMA scheme. Particularly, NOMA-users in a single cell are handled by a BS on the same time, code or frequency channel using different power-values. Figure 1(a) shows the proposed NOMA operation in which two users uses the entire bandwidth simultaneously. While Figure 1(b) shows the conventional OMA operation in which each user uses only one-half of the total bandwidth (BW) which is the addressed problem in this proposed work. NOMA provides wide BW per user whereas OMA provides narrow BW per user. The novelty of NOMA is to intelligently assign the transmit-power (P_t) to different users on the basis of the difference in channel-conditions. The users are identified by their channel-conditions. Specifically, the users with weak channel-conditions are assigned more power by the BS, therefore, such users are enabled to decode their own signals by considering the other users of high power signals as noise. The good channel condition users deploy SIC to decode the signals of weak channel conditions and then decode their

desired signal by removing the other user's signals [6]. It is conclusive from such mechanism that the BS Tx-power is inversely-proportional to the channel-condition in the proposed NOMA scheme. It is due to the fact that the user with weak channel condition is far from the BS and thus the corresponding channel between the BS and UE is weakened by the path-loss. On the other hand, the users that are closer to the BS have good channel condition due to high SNR. That is the fairness scenario which is performed by NOMA. The conventional OMA assigns more power to good channel-condition which is not fairness to users.

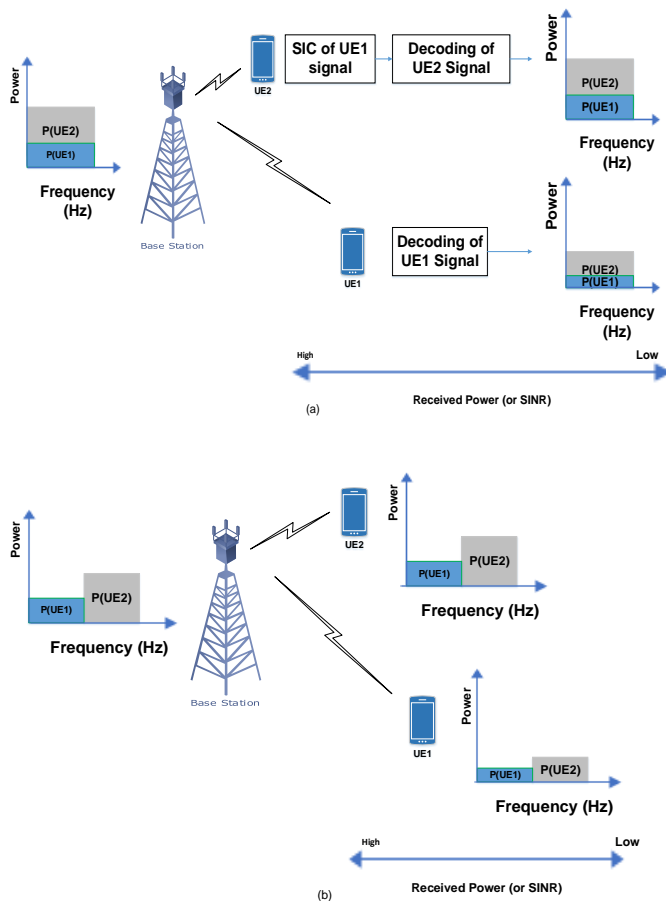


Figure 1. Basic difference between: (a) NOMA, (b) OMA Scheme.

Cooperative Relay communication also gained much research attention due to its dominant features such as spatial-diversity or in other words, antenna diversity, enhanced transmission-reliability, high data-rate and network-coverage. Diversity means that multiple-independent paths are provided to the signal for propagation. Thus, the integration of cooperative-relay with NOMA attracted much research interest to improve the system capacity of 5G communication networks. Particularly, the key benefit of SIC is that the strong-users with good channel-condition have prior knowledge of the signals of weak-users, thus they can act as cooperative-relays to transmit data to the weak user which is an indirect and efficient method. This feature significantly improves the wireless network performance [7].

The UL communication in 4G is performed by the BS using a request-grant paradigm which causes a large overhead and increased latency. To overcome this issue, I propose a grant-free NOMA scheme which is curiously expected in UL-NOMA systems. In this way, the UEs can transmit their data

randomly to the BS where it detects the user's activity via CS-MUD algorithms which deploy sparsity of user activity due to intermittent communication in IoT [8]. For DL communication, many algorithms have been proposed for NOMA systems. A cooperative transmission scheme was proposed in [9], in which the strong-users decode the signals for the weak-users that act as relays to improve the performance of the weak-users. In [10], a NOMA relaying system was proposed based on decode and forward (DF) method over Rayleigh fading-channels. The previous work in [11] shows that the AUSs remain constant in various continuous time-slots, which is not suitable from practical perspective. Furthermore, none of such schemes consider the Rician fading-channel specifically for IoT- intermittent communication, in which users can be sensors or devices with dominant line-of-sight (LoS) communication strategy. Rician fading-channels can model such scenario in an efficient manner.

In this paper, I analyze the performance analysis of the proposed grant-free and cooperative relaying-NOMA for IoT-intermittent communication using a more practical-scenario that in uplink (UL) communication, the AUSs can be changed in several continuous time-slots and deploy a simple and low-complexity based dynamic compressed-sensing (DCS) MUD algorithm to jointly-realize both the user-activity and data-detection. Moreover, as users can join or leave the system randomly, some of the users generally transmit their signals in adjacent time-slots having high probability. This information is used for temporal-correlation of AUSs in several continuous time-slots respectively. The estimated AUS is obtained by the temporal-correlation in the present time-slot which is assumed to be the initial-set for estimating the transmitted signal in the next time-slot. Furthermore, the DL performance in terms of average data-rate is analyzed over Rician fading channels for the cooperative relay NOMA. The mathematical formulation is performed and it is compared with the proposed simulation results for better understanding the associated concepts. The results are also compared with conventional relay system (CRS) to get a clear idea of the dominance of the proposed scheme over the conventional schemes.

The rest of the paper is organized as follows. Section II describes the literature review of the proposed work. The propose system model is explained with mathematical modeling in Section III. The simulation results are provided in Section IV. And finally, Section V concludes the paper.

2. Literature Review

The rapid-growth of 5G IoT and mobile Internet has compelled for 1000x increase in data-traffic by 2020 and require massive-connectivity of sensors, devices or users [12]. Thus, the spectral efficiency (SE) becomes one of the key factor to handle such a big data-traffic. A numerous number of smart devices such as smart phones, tablets and notebooks etc. demand for explosively higher data-rate as well as cell-edge rate. In [13], it is stated that the data-traffic from web browsing, HD-video, multimedia-streaming, social-networking, file-sharing, and software-downloading will be 13x more than that of 2014. Moreover, in [14], it is stated that the IoT will deploy different smart-devices, wearable devices, home appliances, smart-vehicles, sensors that will be interconnected to the Internet to make a web-of-things for the improved living of mankind, which will require more and more data-rate enhancement. From

industrial perspective, the control room will connect various sensors and machines with much low-latency in order to collect important information about the industrial equipment on real-time basis [15].

The Long-Term Evolution (LTE), LTE-Advanced, Vehicle-to-Vehicle (V2V) and WiMAX deploy OFDMA scheme due to fact that orthogonal-access is suitable option to gain better throughput with simple receiver design. But due to the drastic increasing demands for big-data services like HD-video streaming, image-transfer, tele-conferencing, cloud-services, an alternative and optimum solution is required to cope with these demands [16]. The conventional OMA schemes allocate channels to users which are orthogonal in time, frequency or code-domain. The major limiting factor of such OMA schemes is that the maximum number of user accommodation is bounded by the orthogonal sub-carriers and the scheduling mechanism which allocate the time-slot, frequency-band or channel-code to their respective users.

The current research on future 5G network expect that it should achieve a 10x increase in connection-density which means 10^6 -connections/km² [17]. For this issue, an upcoming potential technology called, non-orthogonal multiple access (NOMA) radio technology is proposed which has superior spectral-efficiency (SE) and provide many other merits. NOMA can drastically increase the SE due the fact that it uses the same frequency band for all of its users and it only change their power-levels to differentiate them and perform multiplexing. It also provides massive-connectivity, it is because of the non-orthogonality of the proposed scheme which shows that the number of devices or users are not constrained by the NOMA resources. Furthermore, it provides low-overhead and signal cost as well as low-latency as it does not require request-grant process for connection establishing. The conventional OMA scheme is grant based which send a request of scheduling to the BS and then it performs the required scheduling for the UL communication and send back a grant to the requesting user on DL.

3. System Model

The proposed NOMA DCS-MUD based Uplink (UL) and Cooperative-Relaying based Downlink (DL) system modeling and mathematical analysis is performed in this section.

3.1 Uplink (UL) Transmission

I consider a single-BS UL-NOMA system with K-users and single-antenna aspect is considered with AWGN channels as shown in Figure 2. The k -user transmitted symbol u_k is transformed into a spreading-sequence S_k of length L . Specifically, I consider the overloaded-system scenario in which the number of users are more than the length of the spreading-sequence. i.e. $L < K$. After doing so, all the signals of the active-users are superimposed and then it is transmitted over the L -subcarriers of the OFDM. The signal received by the BS on l -subcarrier can be expressed as:

$$y_l = \sum_{k=1}^K G_{lk} S_{lk} u_k + n_l \quad (1)$$

for $l = 1, 2, 3, \dots, L$

where,

G_{lk} : is the user- k channel-gain on the l -subcarrier,

S_{lk} : is the l -part of S_k ,

n_l : is the l -subcarrier Gaussian noise of zero-mean and unit-variance $\sigma_{n_l}^2$.

All of the above-mentioned variables are independent and identically distributed (i.i.d).

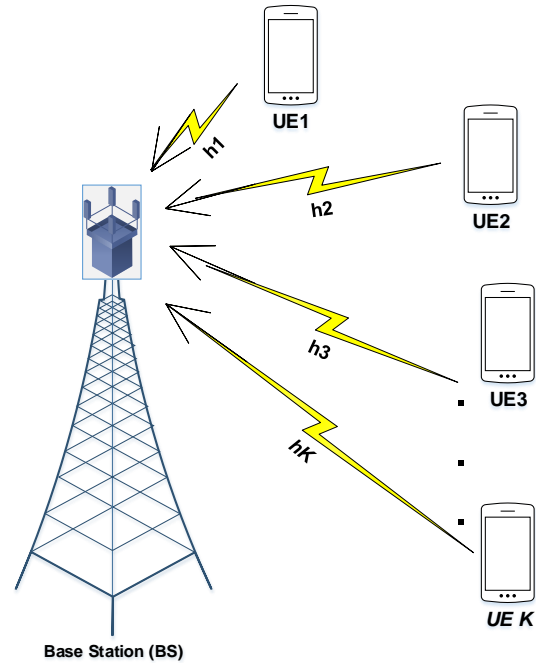


Figure 2. Uplink Channel model for DCS-MUD algorithm.

The combined L -subcarriers signals is written as:

$$y_l = [y_1, y_2, y_3, \dots, y_L]^T \quad (2)$$

The received signal-vector of the combined L -subcarriers signals is then given by:

$$y = Hu + n \quad (3)$$

Where,

$u = [u_1, u_2, u_3, \dots, u_K]^T$: is the signal-vector transmitted for all K -users,

$H = [h_1, h_2, h_3, \dots, h_{lK}]$: is the measurement-matrix of order $L \times K$ and its l -th-row and k -th-column component is h_{lk} which is equal to $G_{lk} S_{lk}$,

$n = [n_1, n_2, n_3, \dots, L]^T$: is the noise-vector having the same attributes as in (1) and follows $\mathcal{CN}(0, \sigma^2 I_N)$.

Specifically, I focus on the recovering of the transmitted signal from the received signals in T -continuous time-slots. Therefore, equation (3) is expressed with the specific time-slot subscript as:

$$y^{(t)} = H^{(t)} u^{(t)} + n^{(t)} \quad (4)$$

For $t = 1, 2, 3, \dots, T$

Where,

$H^{(t)}$: t -th time slot equivalent channel-matrix that can change with different t -slots,

$n^{(t)}$: is the corresponding t -th time-slot noise-vector.

To obtain the support-element of the transmitted signal $u^{(t)}$, let \mathcal{S} -represent the sparsity-level of it, which shows the number of non-zero elements in the transmitted signal. Therefore, the support-element is expressed as follows:

$$\gamma^{(t)} = [k: k \in (1, 2, 3, \dots, K), u_k^t \neq 0] \quad (5)$$

By deploying (5) which provides partial knowledge regarding the received signals, the DCS-MUD joint user-activity and data-detection process can be performed with improved-reliability, which is better than the conventional CS-MUD algorithm. For the detection-reliability analysis, the isometry property (IP) is deployed by the CS for the recovery of signal. To determine the performance-guarantee, the upper-constraint of signal-detection error as well as the successful recovery condition is obtained for the proposed DCS-MUD algorithm. The condition is that the H -matrix will satisfy the IP-property of order \mathcal{S} , if there exists a constant β such that:

$$(1 - \beta)\|u\|_2^2 \leq \|Hu\|_2^2 \leq (1 + \beta)\|u\|_2^2 \quad (6)$$

This is satisfied for all \mathcal{S} -sparse vectors u , so the maximum number of non-zero elements is \mathcal{S} in u . Specifically, the IP-property is satisfied by the Toeplitz-matrix which is based on pseudo-random noise (PN) with a high-probability, which is used in the design of the proposed spreading-matrix S . For determining the residue-signal (ψ), the concept of residue-orthogonality in CS-theory is used on the projection-operator in which an arbitrary-vector and sensing-matrix of full column rank is deployed which is expressed as:

$$\begin{cases} H_l^H \text{resid}(y, H_l) = 0 \\ \|\text{resid}(y, H_l)\|_2 \leq \|y\|_2 \end{cases} \quad (7)$$

Where,

$y \in \mathbb{C}^L$: is the arbitrary-vector (AV), $H_l \in \mathbb{C}^{L \times |\mathcal{M}|}$: is the sensing or sampling-matrix, $\text{resid}(y, H_l) = y - H_l H_l^H y$: is the residue signal, and \mathcal{M} shows the Moore-Penrose inversion of matrix. As AWGN channels are considered, so $H = S$, which means that the measurement-matrix and spreading-matrix are equal. Therefore,

$$H^{(1)} = H^{(2)} = H^{(3)} = \dots = H^{(T)} \triangleq H \quad (8)$$

Also, H satisfy the following conditions:

$$\begin{cases} h_i^H = 1 \\ h_i^H \approx 0, \forall i \neq k \end{cases} \quad (9)$$

By using such IP and residue-orthogonality properties, the residue signal of the proposed DCS-MUD can be obtained as:

$$\|\mathcal{R}^{(i)}\|_2 = \|\text{resid}(y, H_{\hat{\gamma}^{(i)}})\|_2 \quad (10)$$

By using (4) and (5) (10), it follows as:

$$\begin{aligned} &\leq \|\text{resid}(H_{\hat{\gamma}^{(i)}} u_{\hat{\gamma}^{(i)}}, H_{\hat{\gamma}^{(i)}})\|_2 + \|\text{resid}(n, H_{\hat{\gamma}^{(i)}})\|_2 \\ &\leq \|H_{\hat{\gamma}^{(i)}} u_{\hat{\gamma}^{(i)}}\|_2 + \|n\|_2 \\ &\leq \|H_{\hat{\gamma}^{(i)}} u_{\hat{\gamma}^{(i)}}\|_2 + \|n\|_2 \end{aligned} \quad (11)$$

Using (6), it follows:

$$\|\mathcal{R}^{(i)}\|_2 \leq \sqrt{1 + \beta_{2\mathcal{S}+1}} \|u_{\hat{\gamma}^{(i)}}\|_2 + \|n\|_2 \quad (12)$$

Similarly, $\|\mathcal{R}^{(i-1)}\|_2$ can be derived in a similar manner by manipulation of the same equations as:

$$\|\mathcal{R}^{(i-1)}\|_2 \geq \frac{1 - \beta_{2\mathcal{S}+1}}{\sqrt{1 - \beta_{2\mathcal{S}+1}}} \|u_{\hat{\gamma}^{(i-1)}}\|_2 - \|n\|_2 \quad (13)$$

To compare (12) and (13), it requires the relationship between the received signals at i th and i th-1 iterations. First,

the i th-1 iteration support set for updating the estimated-AUS is given by:

$$\check{\gamma}^{(i)} \triangleq \hat{\gamma}^{(i)} \cup \arg \max_k |(h_r)^H \mathcal{R}^{(i-1)}|^2 \quad (14)$$

From (14), the following two-inequalities can be derived:

$$\frac{\|u_{\check{\gamma}^{(i)}}\|_2}{\sqrt{\mathcal{S}}} \leq \frac{2\beta_{2\mathcal{S}+1}}{(1 - \beta_{2\mathcal{S}+1})^2} \|u_{\check{\gamma}^{(i-1)}}\|_2 + \frac{2(1 + \beta_{2\mathcal{S}+1})}{1 - \beta_{2\mathcal{S}+1}} \|n\|_2 \quad (15)$$

$$\|u_{\check{\gamma}^{(i)}}\|_2 \leq \frac{1 + 2\beta_{2\mathcal{S}+1}}{1 - \beta_{2\mathcal{S}+1}} \|u_{\check{\gamma}^{(i-1)}}\|_2 + \frac{2}{1 - \beta_{2\mathcal{S}+1}} \|n\|_2 \quad (16)$$

By putting (15) and (16) into (12) and (13), this give the conditions of termination as:

$$\|\mathcal{R}^{(i)}\|_2 \geq \|\mathcal{R}^{(i-1)}\|_2 \quad (17)$$

The flowchart in Figure 3 illustrates the various important steps performed in the proposed DCS-MUD algorithm.

The iteration will be stopped if the energy-level of the \mathcal{R} is not reduced. From (17), the following result is obtained:

$$\|n\|_2 \geq \frac{\beta_{2\mathcal{S}+1}}{\sqrt{\mathcal{S}+2}} \|u_{\check{\gamma}^{(i-1)}}\|_2 = \frac{\beta_{2\mathcal{S}+1}}{\sqrt{\mathcal{S}+2}} \|u_{\check{\gamma}^{(i)}}\|_2 \quad (18)$$

From (18) it is clear that if the noise-power is greater than the residue active-user signals that is multiplied with a β -coefficient, the iteration-process will be stopped from which the final-estimated AUS is given by:

$$\check{\gamma} = \check{\gamma}^{(i-1)} \quad (19)$$

For the signal reconstruction-error (SRE), the following relationship is used:

$$\|\check{u} - u\|_2 \leq \frac{2 + \sqrt{\mathcal{S} + \beta_{2\mathcal{S}+1} + \beta_{2\mathcal{S}+1}^2}}{\beta_{2\mathcal{S}+1}(1 - \beta_{2\mathcal{S}+1})} \|n\|_2 \quad (20)$$

It clearly shows that the noise-power, IP-property and the \mathcal{S} upper-bound the SRE which is the constrained limit. Table 1 shows the detail of the proposed system parameters which is used for simulations results.

Table 1. Proposed System Specification for DCS-MUD

S. No	Parameter	Symbol	Value
1	Number of users	N	200
2	Number of subcarriers	L	100
3	Number of active users	K	20
4	Common active users	C	15
5	Continuous time slots	T	7
6	Signal-to-Noise Ratio	SNR	14dB

3.2 Downlink (DL) Transmission

The system model for the downlink (DL) performance evaluation is shown in Figure 4.

The DL cooperative-relay NOMA performance analysis is performed over the Rician fading-channels. I consider a typical cooperative-relaying system (CRS) which comprised of a BS source (S), a decode-and-forward (DF) relay (R) which operates in half-duplex manner, i.e. it can receive or transmit signal only one at a time, finally a UE/MS destination (D). The wireless signals paths between each pair of devices are from S -to- D , S -to- R , and R -to- D respectively. The associated channel-coefficients are h_{SD} , h_{SR} and h_{RD} . The

corresponding average-powers are Φ_{SD}^2 , Φ_{SR}^2 and Φ_{RD}^2 respectively. It is clear from the figure that the S -to- D path-loss is greater as compare to the S -to- R path. In Figure 4(a), the conventional CRS send the signal s_1 to the relay (R) and destination (D) in the first time-slot. The relay then sends s_1 to D in the second time-slot.

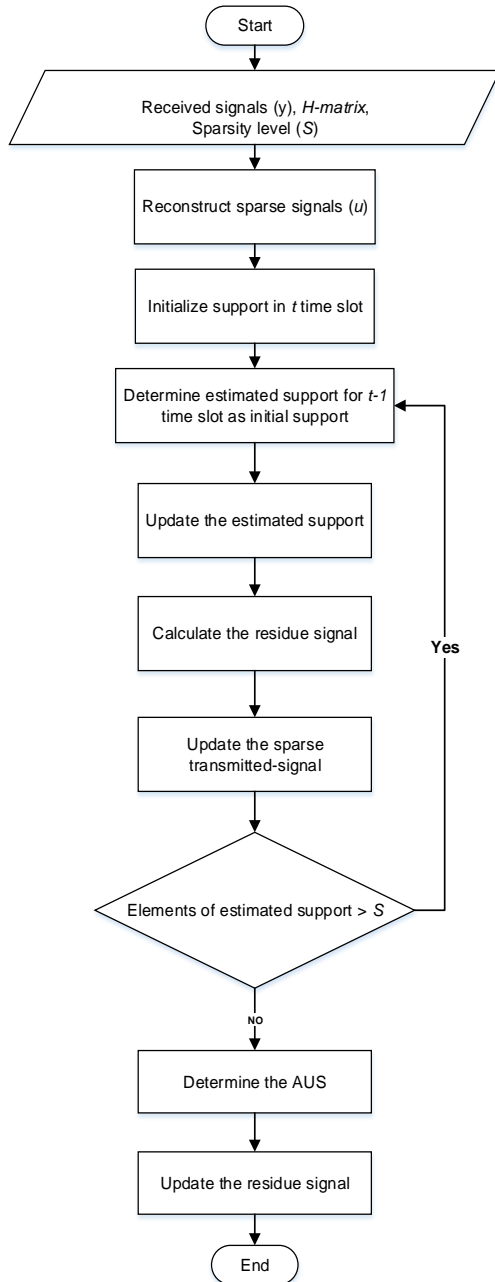


Figure 3. DCS-base MUD flowchart.

Therefore, D receives the same signal s_1 in two time-slots. In Figure 4(b), the source (S) send superposition of two different signals (s_1 and s_2) to the R and D in the first time-slot. So, the benefit of CRS-NOMA is that the destination (D) can receive two different signals in two time-slots which has better throughput than conventional-CRS. The superposition of the two signals that is transmitted to the R and D can be expressed as:

$$S_t = \sqrt{c_1 P_t} s_1 + \sqrt{c_2 P_t} s_2 \quad (21)$$

Where,

s_k : is the k th –signal whose normalized-power is unity;
 P_t : is the total transmit-power;

c_k : is the power-allocation coefficient.

As $\Phi_{SD}^2 < \Phi_{SR}^2$, therefore it is clear that [18]:

$$\begin{cases} c_1 + c_2 = 1 \\ c_1 > c_2 \end{cases} \quad (22)$$

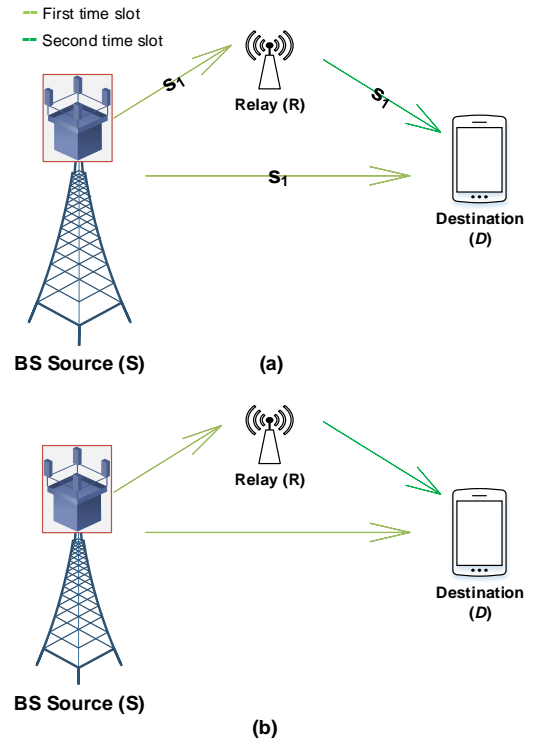


Figure 4. Cooperative relaying system (CRS):
 (a) Traditional CRS, (b) NOMA-CRS.

The signals that are received by the R and D from the source S in the first time-slot are given by:

$$R_{SR} = h_{SR}(\sqrt{c_1 P_t} s_1 + \sqrt{c_2 P_t} s_2) + n_{SR} \quad (23)$$

$$R_{SD} = h_{SD}(\sqrt{c_1 P_t} s_1 + \sqrt{c_2 P_t} s_2) + n_{SD} \quad (24)$$

Where,

n_{SR}, n_{SD} : shows the additive white Gaussian Noise (AWGN) having zero-mean and variance σ^2 .

The destination (D) uses Successive Interference Cancellation (SIC) algorithm to decode the signal s_1 by treating the signal s_2 as noise. The signal-to-interference plus noise ratios (SINRs) for both the signals is expressed as:

$$\eta_{SR}^1 = \frac{|h_{SR}|^2 c_1 P_t}{|h_{SR}|^2 c_2 P_t + \sigma^2} \quad (25)$$

$$\eta_{SR}^2 = \frac{|h_{SR}|^2 c_2 P_t}{\sigma^2} \quad (26)$$

The corresponding SINR for s_1 at D is given by:

$$\eta_{SD} = \frac{|h_{SD}|^2 c_1 P_t}{|h_{SD}|^2 c_2 P_t + \sigma^2} \quad (27)$$

For the second time-slot, only the relay (R) transmits the decoded-signal s_2 to the destination (D) with its full-power P_t , by assuming that R perfectly-decode s_2 in the first time-slot. Therefore, the signal received in the second time-slot at D can be given by:

$$R_{RD} = h_{RD} \sqrt{P_t} s_2 + n_{RD} \quad (28)$$

Where,

n_{RD} : is the noise having the same characteristics as in (23), (24). The corresponding SINR for s_2 is expressed as:

$$\eta_{RD} = \frac{|h_{RD}|^2 P_t}{\sigma^2} \quad (29)$$

From these equations, I will determine the exact and approximated achievable-rates for the proposed CRS-NOMA. The performance analysis over Rician fading-channels is analytically obtained by Taylor expansion of Bessel-function and incomplete Gamma-function. The complexity of the incomplete Gamma-function causes difficulty to obtain the exact values of the required parameters. To cope this issue, I additionally deploy Gauss-Chebyshev (GC) algorithm to make the calculation more feasible.

3.2.1 Exact Average Achievable Rate Analysis

The exact achievable rates of both signals are determined. I assume that $\Gamma_{SD} \triangleq |h_{SD}|^2$, $\Gamma_{SR} \triangleq |h_{SR}|^2$, $\Gamma_{RD} \triangleq |h_{RD}|^2$ and $\rho \triangleq \frac{P_t}{\sigma^2}$. From [19], the achievable rates of both signals are given by:

$$\begin{aligned} r_{S_1} &= \frac{1}{2} \min\{\log_2(1 + \eta_{SD}), \log_2(1 + \eta_{SR}^1)\} \\ &= \frac{1}{2} \log_2\{1 + \min(\Gamma_{SD}, \Gamma_{SR})\rho\} - \frac{1}{2} \log_2\{1 + \min(\Gamma_{SD}, \Gamma_{SR})\rho c_2\} \end{aligned} \quad (30)$$

$$\begin{aligned} r_{S_2} &= \frac{1}{2} \min\{\log_2(1 + \eta_{SR}^2), \log_2(1 + \eta_{RD})\} \\ &= \frac{1}{2} \log_2\{1 + \min(c_2\Gamma_{SR}, \Gamma_{RD})\rho\} \end{aligned} \quad (31)$$

To determine the cumulative distribution function (CDF), I assume $q_1 \triangleq \min(\Gamma_{SR}, \Gamma_{SD})$ and $q_2 \triangleq \min(c_2\Gamma_{SR}, \Gamma_{RD})$. By using [20], the CDF of q_1 is given by:

$$F(q_1) = 1 - C_{SD} C_{SR} \sum_{k=0}^{\infty} \sum_{n=0}^{\infty} \tilde{B}_{SD}(n) \tilde{B}_{SR}(k) n! k! x \gamma(n+1, c_{SD} q_1) x \gamma(k+1, c_{SR} q_1) \quad (32)$$

$$\begin{aligned} (a) \quad & 1 - C_{SD} C_{SR} \sum_{k=0}^{\infty} \sum_{n=0}^{\infty} \tilde{B}_{SD}(n) \tilde{B}_{SR}(k) n! k! e^{-(c_{SD} + c_{SR})q_1} \\ & x \sum_{i=0}^n \sum_{j=0}^k \frac{c_{SD}^i c_{SR}^j}{i! j!} q_1^{i+j} \end{aligned} \quad (33)$$

Where,

$$\begin{aligned} B_{SD}(n) &= \frac{K_{SD}^n (1+K_{SD})^n}{\Phi_{SD}^n (n!)^2}, \quad B_{SR}(k) = \frac{K_{SR}^k (1+K_{SR})^k}{\Phi_{SR}^k (k!)^2}, \\ c_{SD} &= \frac{1+K_{SD}}{\Phi_{SD}}, \quad c_{SR} = \frac{1+K_{SR}}{\Phi_{SR}}, \quad C_{SD} = c_{SD} e^{-K_{SD}}, \quad C_{SR} = \\ & c_{SR} e^{-K_{SR}}, \quad \tilde{B}_{SD}(n) = \frac{B_{SD}(n)}{a_{SD}^{n+1}}, \quad \tilde{B}_{SR}(k) = \frac{B_{SR}(k)}{a_{SR}^{k+1}}, \end{aligned}$$

Here, K represents the Rician factor in these equations. It is worth notable that the second-equality of (33) is used for incomplete Gamma function.

In a similar manner, the CDF of q_2 is expressed by:

$$G(q_2) = 1 - C_{RD} C_{SR} \sum_{k=0}^{\infty} \sum_{n=0}^{\infty} \tilde{B}_{RD}(n) \tilde{B}_{SR}(k) \gamma(n+1, c_{RD} q_2 x \gamma(k+1, c_{SR} c_2 q_2)) \quad (34)$$

$$\begin{aligned} &= 1 - C_{RD} C_{SR} \sum_{k=0}^{\infty} \sum_{n=0}^{\infty} \tilde{B}_{RD}(n) \tilde{B}_{SR}(k) n! k! e^{-(c_{RD} + \frac{c_{SR}}{c_2})q_2} \\ & x \sum_{i=0}^n \sum_{j=0}^k \frac{c_{RD}^i (\frac{c_{SR}}{c_2})^j}{i! j!} q_2^{i+j} \end{aligned} \quad (35)$$

The variables in (35) are defined in the same manner as in (33). The average-achievable rate of signal s_1 is then obtained by putting (32) into (30) as follows:

$$\begin{aligned} r_{S_1} &= \frac{1}{2} \int_0^{\infty} [\log_2(1 + q_1 \rho) - \log_2(1 + q_1 \rho c_2)] dF(q_1) \\ &= \frac{1}{2 \ln(2)} \left[\rho \int_0^{\infty} \frac{1-F(q_1)}{1+q_1 \rho} dq_1 - \rho c_2 \int_0^{\infty} \frac{1-F(q_1)}{1+q_1 \rho c_2} dq_1 \right] \end{aligned} \quad (36)$$

Let suppose that $Q(\rho) = \rho \int_0^{\infty} \frac{1-F(q_1)}{1+q_1 \rho} dq_1$, now putting (33)

in it I get:

$$\begin{aligned} Q(\rho) &= C_{SD} C_{SR} \sum_{k=0}^{\infty} \sum_{n=0}^{\infty} \tilde{B}_{SD}(n) \tilde{B}_{SR}(k) n! k! x \sum_{i=0}^n \sum_{j=0}^k \frac{c_{SD}^i c_{SR}^j}{i! j!} \\ & \int_0^{\infty} \frac{q_1^{i+j} e^{-(c_{SD} + c_{SR})q_1}}{1+q_1 \rho} d(q_1 \rho) \end{aligned}$$

$$\begin{aligned} (b) \quad & C_{SD} C_{SR} \sum_{k=0}^{\infty} \sum_{n=0}^{\infty} \tilde{B}_{SD}(n) \tilde{B}_{SR}(k) n! k! x \sum_{i=0}^n \sum_{j=0}^k \frac{c_{SD}^i c_{SR}^j}{i! j! \rho^{i+j}} \\ & = \int_0^{\infty} \frac{t^{i+j} e^{-\left(\frac{c_{SD} + c_{SR}}{\rho}\right)t}}{1+t} dt \end{aligned} \quad (37)$$

Where (b) is calculated by putting $t = q_1 \rho$, and the integral

$\int_0^{\infty} \frac{t^{i+j} e^{-\left(\frac{c_{SD} + c_{SR}}{\rho}\right)t}}{1+t} dt$ is calculated by the following Lemma.

For $m \in \mathbb{Z}^*$ and $\beta > 0$, it implies that

$$\int_0^{\infty} \frac{t^m e^{-\beta t}}{1+t} dt = e^{\beta} m! \gamma(-m, \beta) \quad (38)$$

Where,

$\gamma(-m, \beta)$: is the incomplete Gamma-function which is substituted for:

$$\gamma(-m, \beta) = \int_{\beta}^{\infty} \frac{e^{-t}}{t^{m+1}} dt \quad (39)$$

Now putting (38) in (37), I get the final exact equation for signal s_1 as follows:

$$r_{S_1} = \frac{1}{2 \ln(2)} [Q(\rho) - Q(\rho c_2)] \quad (40)$$

Where,

$$\begin{aligned} Q(\rho) &= C_{SD} C_{SR} \sum_{k=0}^{\infty} \sum_{n=0}^{\infty} \tilde{B}_{SD}(n) \tilde{B}_{SR}(k) n! k! \\ & x \sum_{i=0}^n \sum_{j=0}^k \frac{(i+j)!}{i! j!} \frac{c_{SD}^i c_{SR}^j}{\rho^{i+j}} e^{-\frac{c_{SD} + c_{SR}}{\rho}} \gamma(-i, -j, \frac{c_{SD} + c_{SR}}{\rho}) \end{aligned} \quad (41)$$

and $Q(\rho c_2)$ shares the same pattern as $Q(\rho)$.

In a similar manner, the exact equation for the signal s_2 is given by:

$$r_{s_2} = \frac{1}{2 \ln(2)} C_{RD} C_{SR} \sum_{k=0}^{\infty} \sum_{n=0}^{\infty} \tilde{B}_{RD}(n) \tilde{B}_{SR}(k) n! k! \\ \times \sum_{i=0}^n \sum_{j=0}^k \frac{(i+j)!}{i! j!} \frac{c_{RD}^i (c_{SR})^j}{\rho^{i+j}} e^{\frac{c_{RD} + c_{SR}}{\rho}} \gamma\left(-i, -j, \frac{c_{RD} + c_{SR}}{\rho}\right) \quad (42)$$

The expression for the exact rate are derived in (40) and (42) but they are still difficult to calculate due its complexity and incomplete Gamma function. So, to overcome this problem, the Gauss-Chebyshev (GC) approximation is used to obtain the approximate achievable rates which are easier to calculate numerically.

3.2.2 Approximate Average Achievable Rate Analysis

The Gauss-Chebyshev (GC) is an Integration method which is deployed in order to make the incomplete Gamma function numerical calculation simple. Figure 5 shows the GC Integration is an accurate method for numerical calculations which converges very-quickly.

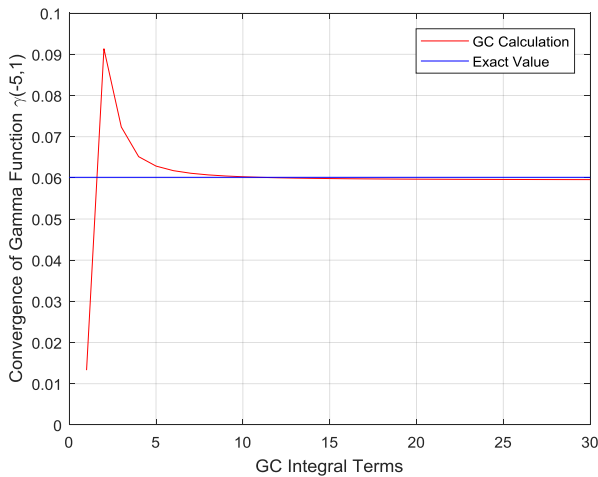


Figure 5. The convergence accuracy of Gauss-Chebyshev approximation.

It is clear from the figure that for the considered incomplete Gamma function $\gamma(-m, \beta) = \gamma(-5, -1)$, the convergence to exact value of 0.0 occur after approximately 15-terms of summation. The intervals in (40) and (42) are infinite whereas the GC-interval is limited which is $[-1, 1]$. Thus, to overcome this issue, I put $t = 2\beta \frac{1}{x} - 1$ in (39) and apply GC-integration to convert the incomplete Gamma-function to the following:

$$\gamma(-m, \beta) = \left(\frac{1}{2\beta}\right)^m \int_{-1}^1 \frac{1}{\sqrt{1-t^2}} (t+1)^{m-1} \\ \times e^{-\frac{2\beta}{t+1} \sqrt{1-t^2}} dt \\ = \left(\frac{1}{2\beta}\right)^m \frac{\pi}{n} \sum_{l=1}^n \left\{ \cos\left(\frac{2l-1}{2n} \pi\right) + 1 \right\}^{m-1} \\ \times e^{-\frac{2\beta}{\cos\left(\frac{2l-1}{2n} \pi\right)+1}} \left| \sin\left(\frac{2l-1}{2n} \pi\right) \right| \quad (43)$$

Where,

n : is the order of approximation.

By putting (43) into (40), finally I get the approximate achievable rate as follows:

$$r_{s_1} = \frac{1}{2 \ln(2)} [Q(\rho) - Q(\rho c_2)] \quad (44)$$

Where,

$$Q(\rho) = C_{SD} C_{SR} \sum_{k=0}^{\infty} \sum_{n=0}^{\infty} \tilde{B}_{SD}(n) \tilde{B}_{SR}(k) n! k! \\ \times \sum_{i=0}^n \sum_{j=0}^k \frac{(i+j)!}{i! j!} \frac{c_{SD}^i c_{SR}^j}{\rho^{i+j}} e^{\frac{c_{SD} + c_{SR}}{\rho}} \left(\frac{1}{2 \frac{c_{SD} + c_{SR}}{\rho}} \right)^{i+j} \\ \times \frac{\pi}{n} \sum_{l=1}^n \left\{ \cos\left(\frac{2l-1}{2n} \pi\right) + 1 \right\}^{i+j-1} \\ \times e^{-\frac{\frac{c_{SD} + c_{SR}}{\rho}}{\cos\left(\frac{2l-1}{2n} \pi\right)+1}} \left| \sin\left(\frac{2l-1}{2n} \pi\right) \right| \quad (45)$$

and $Q(\rho c_2)$ shares the same pattern as $Q(\rho)$.

In a similar manner, the approximate average achievable-rate of the second signal s_2 is expressed as:

$$r_{s_2} = \frac{1}{2 \ln(2)} C_{RD} C_{SR} \sum_{k=0}^{\infty} \sum_{n=0}^{\infty} \tilde{B}_{RD}(n) \tilde{B}_{SR}(k) n! k! \\ \times \sum_{i=0}^n \sum_{j=0}^k \frac{(i+j)!}{i! j!} \frac{c_{RD}^i (c_{SR})^j}{\rho^{i+j}} e^{\frac{c_{RD} + c_{SR}}{\rho}} \left(\frac{1}{2 \frac{c_{RD} + c_{SR}}{\rho}} \right)^{i+j} \\ \times \frac{\pi}{n} \sum_{l=1}^n \left\{ \cos\left(\frac{2l-1}{2n} \pi\right) + 1 \right\}^{i+j-1} \\ \times e^{-\frac{\frac{c_{RD} + c_{SR}}{\rho}}{\cos\left(\frac{2l-1}{2n} \pi\right)+1}} \left| \sin\left(\frac{2l-1}{2n} \pi\right) \right| \quad (46)$$

From the derived approximated achievable rates equations of (44) and (46), the numerical calculations can be easily calculated. Their validation will be verified in the simulation results in the next section.

3.2.3 Outage probability Analysis

The outage probabilities for both symbols of the proposed system are given by:

$$P_{o,s_1} = 1 - e^{-\left(\frac{Y_{th}}{\rho \Phi_{SD}}\right)} - \frac{\Phi_{RD} e^{-\frac{Y_{th}}{\rho} \left(\frac{1}{\Phi_{RD}} + \frac{1}{\Phi_{SR}}\right)}}{\frac{Y_{th} \Phi_{SD} + \Phi_{RD}}{\Phi_{RD} e^{-\frac{Y_{th}}{\rho} \left(\frac{1}{\Phi_{RD}} + \frac{1}{\Phi_{SR}} + \frac{1}{\Phi_{SD}}\right)}}} + \quad (47)$$

$$P_{o,s_2} = 1 - \frac{\Phi_{RD}}{Y_{th} \Phi_{SD} + \Phi_{RD}} e^{-\left(\frac{Y_{th}}{\rho \Phi_{SD}} - \frac{Y_{th}}{\rho \Phi_{RD}}\right)} \quad (48)$$

Table 2 shows the detail of the proposed system parameters which is used for simulations results.

Table 2. Proposed System Specification for DL CRS-NOMA

S. No	Parameter	Symbol	Value
1	Rician distribution parameter	θ	$\frac{\pi}{2}$
2	Rician factor (SR, RD)	K	6
3	Average powers (SR, RD)	Φ	36

4	Average SD-link power	Φ_{SD}	9
5	Power allocation coefficient	c_2	0.9
6	Signal-to-Noise Ratio	SNR	100dB

4. Simulation Results

The simulation results are provided to validate our analytical formulations. Figure 6 shows the comparison of the conventional CS-MUD and the proposed DCS-MUD algorithms. I consider 200% overloading factor by deploying 200 users, 100 subcarriers. Specifically, 7 number-of continuous time-slots are considered according to LTE-A system perspective with 20 number of active users.

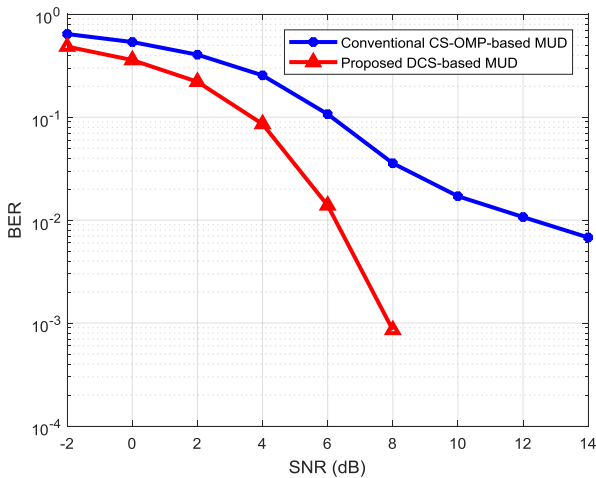


Figure 6. BER comparison of conventional CS-MUD and proposed DCS-MUD in UL grant-free NOMA with 200% overloading factor.

It is clear that by observing both schemes at $BER = 10^{-2}$, the proposed algorithm achieve approximately about 6 dB SNR-gains over the conventional CS-MUD scheme due to the deployment of temporal correlation of AUSs within several continuous time-slots. Moreover, the proposed DCS-MUD performance gets more superior and dominant for high SNR. The gap between the proposed and the conventional schemes gets larger when SNR is increasing, due to the fact that the proposed scheme BER decreases with increasing SNR whereas, the conventional scheme BER does not decrease for high SNR.

Figure 7 shows the average achievable sum-rate comparison of the both signals s_1 and s_2 using the proposed CRS-NOMA. The sum-rate is observed against the power-allocation coefficient c_2 of signal s_2 . It is clear from the figure that when c_2 increases, the s_2 rate increases and the s_1 rate decreases. It is due to the fact that s_2 gets more-power. Furthermore, when the coefficient c_2 increases from 0.1 to 0.5, the s_1 rate decreases from 1.719 bits/s/Hz to 0.491 bits/s/Hz, whereas the s_2 rate increases from 4.127 bits/s/Hz to 5.237 bits/s/Hz.

Figure 8 shows the comparison of the achievable sum-rates of the conventional-CRS and the proposed CRS-NOMA systems. It is clear from the figure that the proposed CRS-NOMA achieves higher sum-rate for increasing SNR than the conventional-CRS. Moreover, as s_1 gets low-power so it has poor achievable rate than s_2 which gets more-power.

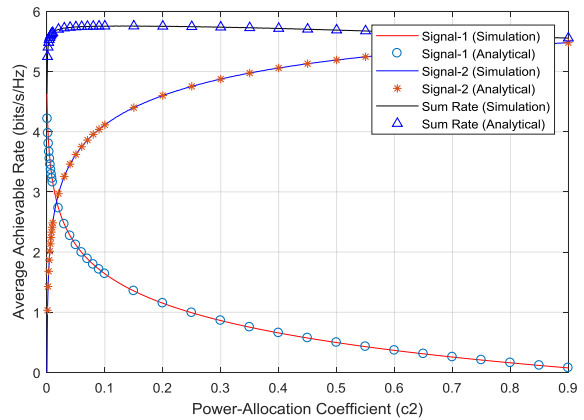


Figure 7. Comparison of sum-rates for both signals in CRS-NOMA schemes under Rician fading-channels.

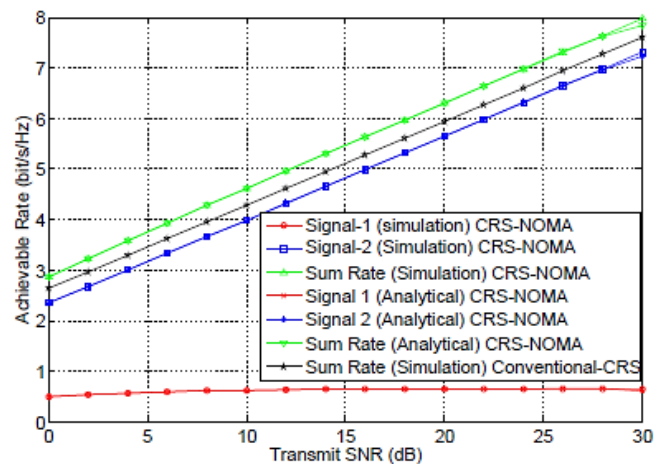


Figure 8. Sum rate comparison of the proposed CRS-NOMA and the conventional-CRS against the SNR.

Figure 9 shows the performance comparison of the outage probability versus the transmit SNR with different power levels. It is clear from the figure that, the simulation results perfectly match the analytical results. Moreover, the outage probability improves for the first symbol as the quality of the $R-D$ link increases. Furthermore, corresponding curves gap decreases when the power levels between the $R-D$ link increases from 10 to 50, which means that its effect becomes negligible. The high-SNR approximations are close at moderate-SNR and it becomes exact at high SNR regime.

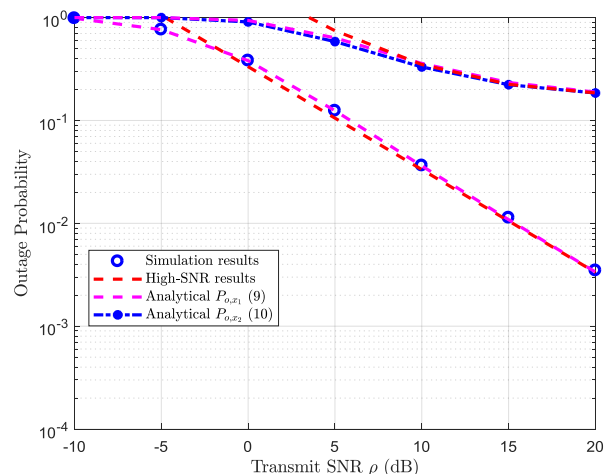


Figure 9. Comparison of the proposed and analytical results in terms of outage probability against the transmit SNR with different power levels.

different values of power levels Φ_{RD} and Φ_{SR} and SINR remains constant and 10 and 0dB.

Figure 10 shows the achievable rate comparison of the simulations, analytical and the high SNR approximation against the transmit SNR. It is clear from the figure that, the simulation result is consistent with the analytical results. The proposed scheme performance is better than CRS-OMA at low and high SNRs. It is because of the SIC algorithm which is used at the destination, which facilitates the second symbol transmission during the second time-slot. Moreover, the fading gain of the first symbol is also improved due the relay node which shortens the R - D link distance.

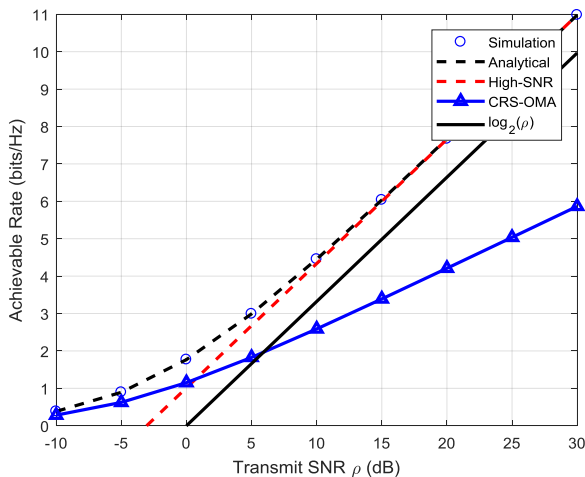


Figure 10. Achievable rate comparison of the proposed CRS-NOMA with conventional OMA in against the transmit SNR with different values of power levels Φ_{RD} and Φ_{SR} remains constant at 10.

5. Conclusions

This paper focuses on the uplink (UL) grant-free NOMA and downlink (DL) DCS-MUD techniques. The proposed DCS-MUD performs joint user-activity and data-detection in several continuous time-slots. The conventional CS-MUD independently detect user in each time-slot whereas our proposed DCS-MUD performs it simultaneously. It is because of deploying the estimated AUS in current time-slot as the reference set to estimate the transmitted-signal in the next time-slot. The proposed DCS-MUD algorithm has low computational-complexity in each iteration. As compare to the conventional CD-MUD algorithm which does not have the partial-known support feature, the proposed DCS-MUD algorithm has lower complexity than the CS-MUD scheme. The downlink CRS-NOMA scheme uses GC-integration which converge quickly to achieve higher sum-rate as compare to conventional-CRS system. The outage probability of the proposed system is also analyzed in term of transmit SNR. The analysis validated that the higher average power of the R - D path improves the system performance. Finally, the proposed scheme shows better overall performance than the conventional OMA scheme in the entire SNR regime.

References

- [1] A. Rehman, S. Rehman, I. Khan, M. Moiz and S. Hasan, "Security and privacy issues in IoT," International journal of communication networks and information security, Vol. 8, No. 3, 2016.

- [2] M. Khan, M. Ashraf, H. Zafar, and T. Ahmad, "Enhanced handover mechanism in long term evolution (LTE) networks," International journal of communication networks and information security, Vo. 9, No. 1, 2017.
- [3] Y. Aun, S. Manickam and S. Karuppayah, "A review on features' robustness in high diversity mobile traffic classifications," International journal of communication networks and information security, Vol. 9, No. 2, 2017
- [4] Xin Su, H. Yu, W. Kim, C. Chol, and D. Choi, "Interference cancellation for non-orthogonal multiple access used in future wireless mobile networks," EURASIP Journal on wire. comm. 2016:231.
- [5] M. Basharat, W. Ejaz, M. Naeem, and A. M. Khattak, "A survey and taxonomy on nonorthogonal multiple-access schemes for 5G networks," Tans. Emerging Tel. Tech. Wiley; e3202, 2017.
- [6] Z. Ding, L. Dai, and H. Vincent Poor, "MIMO-NOMA design for small packet transmission in the Internet of Things," IEEE access Vol. 4, pp. 1393–1405, 2016.
- [7] X. Yue, Y. Liu, S. Kang, and A. Nallanathan, "Performance analysis of NOMA with fixed gain relaying over nakagami- m fading channels," IEEE access Vol. 5, pp. 5445–5454, 2017.
- [8] J. B. Kim and I. H. Lee, "Non-orthogonal multiple access in coordinated direct and relay transmission," IEEE Commun. Lett., vol. 19, No.11, pp. 2037–2040, 2015.
- [9] Z. Ding, M. Peng and H. V. Poor, "Cooperative non orthogonal multiple access in 5G systems," IEEE Commun. Lett., vol. 19, No. 8, pp. 1462–1465, 2015.
- [10] J. B. Kim and I. H. Lee, "Capacity analysis of cooperative relaying systems using non-orthogonal multiple access," IEEE Commun. Lett., vol. 19, No. 11, pp. 1949–1952, 2015.
- [11] B. Wang, L. Dai, T. Mir, and Z. Wang, "Joint user activity and data detection based on structured compressive sensing for NOMA," IEEE Commun. Lett., vol. 20, No. 7, pp. 1473–1476, 2016.
- [12] L. Dai, B. Wang, Y. Yuan, S. Han, C. Lin I, and Z. Wang, "Non-orthogonal multiple access for 5G: solutions, challenges, opportunities, and future research trends," IEEE Comm. Mag., Sep. 2015.
- [13] E. Bjornson, J. Hoydis, M. Kountouris and M. Debbah, "Massive MIMO systems with non-ideal hardware: energy efficiency, estimation, and capacity limits," IEEE Trans. On Inf. Theory, Vol. 60, No. 11, pp. 7112–7139, 2014.
- [14] C. Lai, H. Li, X. Liang, R. Lu, K. Zhang, and X. Shen, "CPAL: A conditional privacy-preserving authentication with access linkability for roaming service," IEEE Internet Things J., Vol. 1, No. 1, pp. 2327–4662, 2014.
- [15] M. Condoluci, M. Dohler, G. Araniti, A. Molinaro, and J. Sachs, "Enhanced radio access and data transmission procedures facilitating industry-compliant machine-type communications over LTE-based 5G networks," IEEE Wireless Commun., Vol. 23, No. 1, pp. 56–63, 2016.
- [16] NGMN 5G White Paper, NGMN Alliance, Feb. 2015.
- [17] F. Boccardi, R. W. Heath, A. Lozano, T. L. Marzetta, and P. Popovski, "Five disruptive technology directions for 5G," IEEE Commun. Mag., Vol. 52, No. 2, pp. 74–80, 2014.
- [18] Y. Saito, A. Benjebbour, Y. Kishiyama, and T. Nakamura, "System-level performance evaluation of downlink non-orthogonal multiple access (NOMA)," in Proc. IEEE Annu. Symp. PIMRC, London, U.K., pp. 611–615, 2013.
- [19] J.-B. Kim and I.-H. Lee, "Capacity analysis of cooperative relaying systems using non-orthogonal multiple access," IEEE Commun. Lett., Vol. 19, No. 11, pp. 1949–1952, 2015.
- [20] M. R. Bhatnagar, "On the capacity of decode-and-forward relaying over rician fading channels," IEEE Commun. Lett., Vol. 17, No. 6 , pp. 1100–1103, 2013.